Renewable Energy and Power Quality Journal
https://repqj.com/index.php/repqj/index
RE&PQJ, Vol. 23, No. 3, 2025

Using Unmanned Aerial Vehicle Inspection Digital Orthophotos and Search Tree Algorithm to Improve the Accuracy of Power Line Defect Recognition

Lei Wei[1,*], Junchen Guo[2]

[1]NARI Nanjing Control System Co. Ltd, Nanjing City, 211106, Jiangsu Province, China
[2]College of Information Science and Engineering, Hohai University, Changzhou City, 213000, Jiangsu Province, China
[*]Corresponding author email: dingj_01@163.com

Abstract. The existing power line defect recognition method relies on traditional image processing technology, which has the disadvantages of slow processing speed, low recognition accuracy, and inability to effectively deal with complex scenes, resulting in frequent false positives and false negatives. To solve this problem, this paper combined the unmanned aerial vehicle (UAV) inspection digital orthophotos and the search tree algorithm to realize the automatic recognition method of power line defects. Firstly, the paper used UAV to obtain high-resolution power grid orthophotos. After geometric correction, the image is divided into multiple regions of interest using image segmentation technology. Then, the paper used U-Net CNN (convolutional neural network) for pixel-level semantic segmentation to recognize potential defect areas. Unlike prior UAV-based defect detection frameworks that primarily utilize standard convolutional networks, the integration of U-Net with A-star search leverages semantic segmentation and path optimization to enhance defect localization accuracy. In the U-Net network, the learning ability of deep features is enhanced by residual blocks and skip connections. The A-star search algorithm is used to search the path of the defect area output by U-Net, and the heuristic function is used to optimize the positioning of suspected defects. The geometric morphology of the power line is analyzed by combining Hough transform, and the straight line and curve features are extracted to improve the recognition ability of power line structure defects. Finally, the paper integrated and optimized through multi-scale analysis and post-processing technology to precisely locate the defect type and location. Experimental results show that the proposed method achieves a maximum accuracy of 98.2% in power grid line defect recognition, and the minimum positioning accuracy reaches 2 mm. Compared to the Canny edge detection method with an accuracy of 82.3% and the baseline U-Net model averaging 92.6%, this approach integrating U-Net with A-star search demonstrates superior recognition precision. Despite its high accuracy, the method faces challenges related to computational overhead under real-time constraints, variable performance across adverse weather conditions, and reliance on extensive annotated datasets, providing efficient and precise automation technical support for power grid inspection and improves power grid operation and maintenance's the intelligent level.

Key words. UAV Inspection, Digital Orthophotos, U-Net Convolutional Neural Network, A-star Search Algorithm, Geometric Feature Extraction

1. Introduction

With the continuous development of power systems, the inspection and maintenance of power grid lines are becoming more important. The real-time detection of power line defects directly impacts the operational safety and reliability of power grids, mitigating risks of widespread outages and substantial economic losses. Power lines [1,2], as the core facilities of power grids [3,4], carry a large amount of power transmission [5,6] tasks. Once a fault occurs [7,8], it may lead to large-scale power outages [9,10] and equipment damage, and even cause serious economic losses and safety hazards. How to efficiently and accurately detect defects [11] and abnormal problems in power grid lines has become a research focus in the power industry [12,13]. Traditional power grid line [14] inspection methods mainly rely on manual inspection and automation technology based on simple image processing. These methods have many limitations, which are particularly prominent under the requirements of high-precision and high-efficiency automatic recognition. Manual inspection is time-consuming and labor-intensive, and is easily affected by factors such as the experience of inspectors, weather, and working environment, resulting in uncertainty in inspection results and missed detection. Although the automation method based on traditional image processing [15,16] technology has improved the inspection efficiency to a certain extent, it is still difficult to provide high-precision recognition and positioning

when faced with the complex terrain environment, different lighting conditions, and diverse defect forms of power grid lines. Traditional image processing methods usually lack sufficient capture of image details and cannot effectively deal with noise interference and complex backgrounds. The paper's method addresses these limitations by leveraging high-resolution UAV orthophotos to mitigate the impact of environmental noise, varying lighting conditions, and diverse defect morphologies, thereby enhancing defect detection reliability in practical power grid inspection scenarios. Therefore, they cannot meet the high-precision and high-robustness requirements in practical applications. Although the existing deep learning (DL) [17,18] models have made significant progress image recognition, and power grid defect recognition [19,20], how to make full use of the high-resolution orthophotos obtained by UAV [21,22] to accurately and quickly locate defects still needs further research [23,24].

With the continuous advancement of UAV technology and image processing technology, the efficiency and accuracy of power inspection have been significantly improved. Prior research has leveraged convolutional neural networks to detect insulator defects, hybrid deep learning frameworks to identify damaged power lines, and optimization strategies like the Golden Eagle optimizer to refine UAV path planning, yet these methods often face challenges in balancing computational efficiency with precision across diverse inspection environments. Yang [25] et al. used DL and transfer learning models to propose a new recognition algorithm for the defect of missing caps on high-voltage transmission line insulators, achieving efficient and preicse detection in complex environments. As the requirements for path planning [26,27] for inspection tasks become increasingly stringent, researchers are committed to improving inspection efficiency and path planning accuracy through optimization algorithms. Pan [28] et al. used the Golden Eagle optimizer that incorporates personal example learning and mirror reflection learning to optimize UAV power inspection path planning and achieve efficient path generation and smoothing. To further improve the analysis efficiency and accuracy of inspection data [29,30], researchers focus on the application of image processing technology, especially innovations in noise suppression and data visualization. Liu [31] et al. used the power corridor visualization technology of data acquisition layer image denoising to visualize UAV line inspection data, improve inspection accuracy, and verify the significant advantages of this method in practical applications. These studies have achieved remarkable results, but the robustness and practicality of the algorithms in high-precision and large-scale power inspection tasks [32,33] still need to be further improved.

In power line defect recognition, people have proposed a variety of technical solutions to improve the accuracy and real-time performance of defect detection. Liu [34] et al. reviewed insulator defect detection using DL methods, pointed out that current research has shortcomings such as inaccurate insulator defect positioning, insufficient robustness of detection models in complex scenes, and limited model performance improvement due to small-scale insulator defect data, and looked forward to future development directions. To overcome these limitations, people continue to explore innovative methods that integrate multiple detection methods to improve the accuracy and reliability of defect recognition [35,36]. Zhu [37] et al. combined online and offline partial discharge (PD) diagnosis methods to improve the recognition accuracy of cable defects in distribution networks and verified the effectiveness of this method in practical applications. With the development of the Internet of Things [38] technology, the application of edge computing has gradually shown its advantages in real-time data processing and fault diagnosis. Han [39] et al. constructed a GRU-VAE (Gated Recurrent Unit-Variational Auto-Encoder) defect recognition model and applied an edge computing architecture to achieve real-time defect detection of electromechanical equipment at the edge of the power grid, providing a new path for electromechanical equipment defect detection. These studies have provided innovative technical solutions for power grid line defect recognition, but in practical applications, they still face challenges such as insufficient model stability, limited data samples, and real-time detection capabilities.

To solve this problem, this paper adopts an automated power grid line defect recognition method that combines UAV inspection digital orthophotos with DL technology. U-Net is employed for its superior performance in pixel-level semantic segmentation of high-resolution images, outperforming alternatives like Mask R-CNN or Transformer-based architectures in preserving spatial details critical for small defect detection, while the A-star algorithm is integrated for its efficiency in path optimization, surpassing Dijkstra's exhaustive search and genetic algorithms' computational complexity in dynamic defect localization. Using UAV to obtain high-resolution power grid orthophotos avoids the shortcomings of traditional manual inspections and simple image processing methods, and combines efficient image processing algorithms to improve the accuracy and efficiency of power grid line defect recognition. This paper geometrically corrects the high-resolution orthophotos taken by UAV to ensure the accuracy of the spatial information of the image. Then, the image is divided into multiple regions of interest using image segmentation technology. This process optimizes the subsequent recognition of defective areas by extracting features from the image. The U-Net convolutional neural network is used to perform pixel-level semantic segmentation on these areas to precisely recognize defective areas in the power grid line. The U-Net network has a strong feature extraction capability and performs well in processing high-resolution images. It can effectively recognize small defects and anomalies in complex scenes. To further improve the positioning accuracy of defects, this paper applies the A-star search algorithm to finely locate the suspected defect areas recognized. The algorithm

optimizes the search path by setting heuristic functions and dynamic cost functions, thereby precisely locating the defect location and avoiding false positives. Finally, the geometric morphology of the power grid line is analyzed in combination with the Hough transform to improve the recognition ability of power line structural defects and further improve the overall recognition effect. In the post-processing stage of the results, the interference of environmental noise is reduced through multi-scale analysis and image fusion technology, and precise defect type and location positioning is achieved. This method significantly improves the accuracy of power grid line defect recognition, and improves the adaptability to complex scenes and diversified defects, and promotes the automation and intelligent process of power grid inspection.

2. Defect Recognition Method

This paper introduces the overall process of power grid line defect recognition in detail, covering all steps from UAV acquisition of high-resolution images to the final output of defect recognition results. The process includes image acquisition and preprocessing, image segmentation and defect area recognition, defect positioning and path search, geometric morphology analysis and defect optimization, as well as post-processing and result optimization. Each link is carefully designed to ensure recognition accuracy and system robustness. Through the coordinated optimization of each link, this paper strives to achieve efficient and accurate detection of power grid line defects. The defect recognition process is shown in Figure 1.

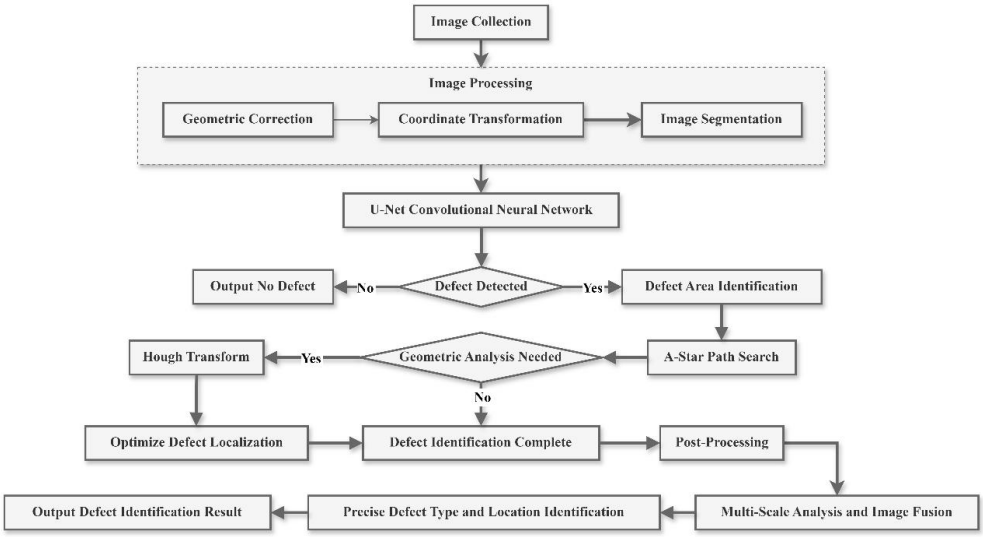

Figure 1. Power grid line defect recognition process.

A. Image Acquisition and Preprocessing

Acquiring high-resolution digital orthophotos is the basis for power grid defect recognition. This paper uses UAV to collect images at different angles and distances. The collected image style is shown in Figure 2.

Figure 2. Collected image style.

After the image is acquired, geometric correction is performed to eliminate image deformation caused by UAV flight posture, camera angle, and lens distortion. The key to geometric correction is to establish a precise mapping between image coordinates and geographic coordinates through ground control points (GCPs). The relationship between the point (x_i, y_i) in the image and its corresponding geographic coordinate (X_i, Y_i) is represented by a transformation matrix:

$$\begin{bmatrix} x_i \\ y_i \end{bmatrix} = \begin{bmatrix} a & b \\ c & d \end{bmatrix} \begin{bmatrix} X_i \\ Y_i \end{bmatrix} + \begin{bmatrix} e \\ f \end{bmatrix} \quad (1)$$

In the Formula (1), a, b, c, d are the parameters of the transformation matrix, and e and f are the translation amounts. These parameters are estimated by the least squares method to minimize the error between the actual GCP and the transformed point.

After geometric correction, coordinate transformation is performed to map the image pixel coordinates to the UTM (Universal Transverse Mercator) coordinate system

to ensure the consistency of the image in geographic space. Assuming that the pixel coordinate of a point in the image is (x, y), and its geographic coordi0 (X, Y) is:

$$\begin{bmatrix} X \\ Y \end{bmatrix} = \mathbf{T} \begin{bmatrix} X \\ y \end{bmatrix} \quad (2)$$

In the Formula (2), $\mathbf{T}$ is the projection transformation matrix, which is responsible for converting the image coordinate system to the geographic coordinate system. During the conversion process, the parameters of $\mathbf{T}$ are determined by the actual measured GCP points to ensure high-precision docking between the image and the geographic coordinate system.

After geometric correction and coordinate transformation, image optimization and data enhancement are required to improve the image quality and the accuracy of subsequent defect detection. Image optimization improves the defect recognition accuracy by enhancing the detail information; data enhancement improves the model robustness through image transformation and adapts to different environmental changes. The first step of image optimization is histogram equalization, which adjusts the pixel distribution to make the brightness range uniform and the pixel value range $[0, L-1]$, where L is the total number of pixel values. The goal of histogram equalization is to map the pixel value $I(x, y)$ of the input image to the new pixel value $I'(x, y)$ through the mapping function T, so that the pixel value distribution of the output image is more uniform. The mapping process is:

$$I'(x, y) = T(I(x, y)) = (L-1) \cdot \sum_{i=0}^{I(x,y)} h(i) \Big/ N \quad (3)$$

In the Formula (3), N is the total number of pixels in the image, and $h(i)$ is the histogram of the original image. This method can effectively improve the contrast of the image, enhance the details, and facilitate the subsequent extraction of defect areas.

The application of data augmentation methods helps to generate diverse training samples, avoid overfitting and enhance the adaptability of the model in complex environments. Data augmentation operations are generally implemented through affine transformations, which include translation, rotation, scaling, etc. It is assumed that the translation transformation matrix of the image is:

$$\mathbf{F} = \begin{bmatrix} 1 & 0 & \Delta x \\ 0 & 1 & \Delta y \\ 0 & 0 & 1 \end{bmatrix} \quad (4)$$

In the Formula (4), Δx and Δy represent the horizontal and vertical translation of the image, respectively. Through this matrix, each pixel position (x, y) in the image is converted to a new position (x', y'):

$$\begin{bmatrix} x' \\ y' \\ 1 \end{bmatrix} = \mathbf{T} \begin{bmatrix} x \\ y \\ 1 \end{bmatrix} \quad (5)$$

For rotation transformation, assuming that the rotation angle is θ, the rotation matrix is:

$$\mathbf{R} = \begin{bmatrix} \cos\theta & -\sin\theta \\ \sin\theta & \cos\theta \end{bmatrix} \quad (6)$$

The pixel position after rotation is:

$$\begin{bmatrix} x' \\ y' \end{bmatrix} = \mathbf{R} \begin{bmatrix} x \\ y \end{bmatrix} \quad (7)$$

The equation for scaling transformation is:

$$\begin{bmatrix} x' \\ y' \end{bmatrix} = \mathbf{S} \begin{bmatrix} x \\ y \end{bmatrix} \quad (8)$$

In the Formula (8), $\mathbf{S}$ is the scaling matrix, which represents the scaling ratio of the image in the horizontal and vertical directions.

B. Image Segmentation and Defect Area Recognition

This paper uses the U-Net convolutional neural network for image segmentation, aiming to accurately separate potential defect areas from high-resolution digital orthophotos acquired by UAV. The U-Net network has an encoder and decoder structure. The encoder is used to extract deep features of the image, and the decoder reconstructs the spatial resolution of the image through upsampling operations, and finally outputs the category probability of each pixel. The network structure of U-Net consists of multiple convolutional layers and pooling layers. The U-Net architecture employs a symmetric encoder-decoder framework with four downsampling layers in the encoder, each featuring two 3x3 convolutions followed by a 2x2 max-pooling operation, and corresponding upsampling layers in the decoder that integrate feature maps via skip connections to preserve spatial details. The network extracts local features of the image through convolution operations and gradually increases the receptive field to capture the global information of the image. To improve the network's ability to learn deep features, residual blocks and jump connections are used in U-Net. The residual block

applies shortcut connections to alleviate the gradient vanishing problem and ensure smooth information flow during training. The jump connection directly connects the feature map in the encoder with the upsampling result in the decoder, so that the network can retain more detailed information and improve the accuracy of the segmentation results.

During the training process, the image data is standardized and uniformly adjusted to the same size. Data augmentation technology is widely used in the construction of training sets. By rotating, scaling, cropping, and other operations on the original image, the diversity of training samples is increased, and the generalization ability of the model is improved. In terms of loss function, the cross-entropy loss function is used to measure the difference between the predicted result and the true label, and the optimization goal is to minimize the loss function. Assuming that the network prediction output is $\hat{y}_i$ and the true label is y_i, the cross-entropy loss function is defined as:

$$\mathcal{L} = -\sum_{i=1}^{N} \left[y_i \log\left(\hat{y}_i\right) + \left(1 - y_i\right) \log\left(1 - \hat{y}_i\right) \right] \quad (9)$$

N is the total number of pixels in the image. To further improve the segmentation accuracy, the Dice coefficient is also used as an evaluation indicator in the training of U-Net. This coefficient measures the overlap between the predicted segmentation result and the true segmentation result, and is defined as:

$$\text{Dice} = 2\sum_{i=1}^{N} y_i \hat{y}_i \Big/ \sum_{i=1}^{N} y_i + \sum_{i=1}^{N} \hat{y}_i \quad (10)$$

To ensure the best training effect, this paper gradually optimizes multiple key hyperparameters. The hyperparameters and initial values, first optimization, second optimization, and final values are shown in Table 1.

Table 1. U-Net model hyperparameter optimization process.

Parameter	Initial Value	First Optimization	Second Optimization	Final Value
Learning Rate	0.001	0.0005	0.0003	0.0001
Batch Size	16	32	32	64
Number of Layers	4	5	5	5
Kernel Size	3x3	3x3	5x5	5x5
Activation Function	ReLU	LeakyReLU	LeakyReLU	LeakyReLU
Optimizer	Adam	Adam	Adam	Adam
Loss Function	Cross-Entropy	Cross-Entropy	Cross-Entropy	Cross-Entropy
Data Augmentation	0.2	0.3	0.4	0.5

In the output results of image segmentation, noise and discontinuity in small defect areas are common problems. To solve this problem, this paper uses morphological operations as a post-processing step to further optimize the segmentation results. Morphological operations are a processing method based on image shape, which is often used in binary image processing. They can remove noise and fill the holes in the defect area, thereby enhancing the connectivity of the target area. The erosion operation is to scan the image through a structural element to remove small areas and noise in the image. Here, it is used to remove small pseudo-defects. This operation shrinks the white area in the image and eliminates irregular or isolated noise. Assuming that the structural element is S, the erosion operation E is:

$$E(I,S) = \min_{(x,y)\in S} I\left(x + x_s, y + y_s\right) \quad (11)$$

In the Formula (11), $\left(x_s, y_s\right)$ is the offset of the structural element. The erosion operation scans the image and the structural element, takes the minimum value of the intersection area, and removes the area in the image that is smaller than the structural element to reduce noise.

The opposite of the erosion operation is the dilation operation. The dilation operation expands the target area in the image, making the small defect area more prominent, and then fills the holes in the area. The dilation operation is usually used to enhance the connectivity of the target area. In the dilation operation, the structural element is convolved with the image to expand the bright area in the image. The dilation operation D is:

$$D(I,S) = \max_{(x,y)\in S} I\left(x + x_s, y + y_s\right) \quad (12)$$

This operation is similar to corrosion, except that the dilation operation takes the maximum value in the region, which expands the target region in the image.

Combining corrosion and dilation operations, an opening operation and a closing operation are formed, which are used to remove small noise points and fill small holes respectively. The opening operation usually performs corrosion first and then dilation operation, which effectively removes small noise points and maintains the shape of the target region. The closing operation performs dilation first and then corrosion, which is

mainly used to fill holes in the region. Through these morphological operations, the output image of the U-Net model is further optimized, and the noise is removed. The defective area is smoothed and filled, and the continuity and accuracy of the defective area are ensured. The optimized image is used as the input for subsequent defect positioning and path search, providing clearer and more precise defective area information, and providing a reliable basis for the precise recognition and positioning of power grid line defects.

C. Defect Positioning and Path Search

The precise defect positioning is one of the key links during power grid line defect recognition. To achieve this goal, this paper uses the A-star search algorithm to precisely locate the suspected defect area output by the U-Net network. The A-star algorithm is a path search algorithm based on a heuristic function. By optimizing the path search process, it can efficiently locate the defect area in complex scenes. In this process, the image segmentation results are used to delineate the suspected defect area according to the grayscale and edge information of the image. These areas serve as the search space of the A-star algorithm and become the starting point for finding the optimal path. Figure 3 shows the application process of the A-star search algorithm in power line defect location.

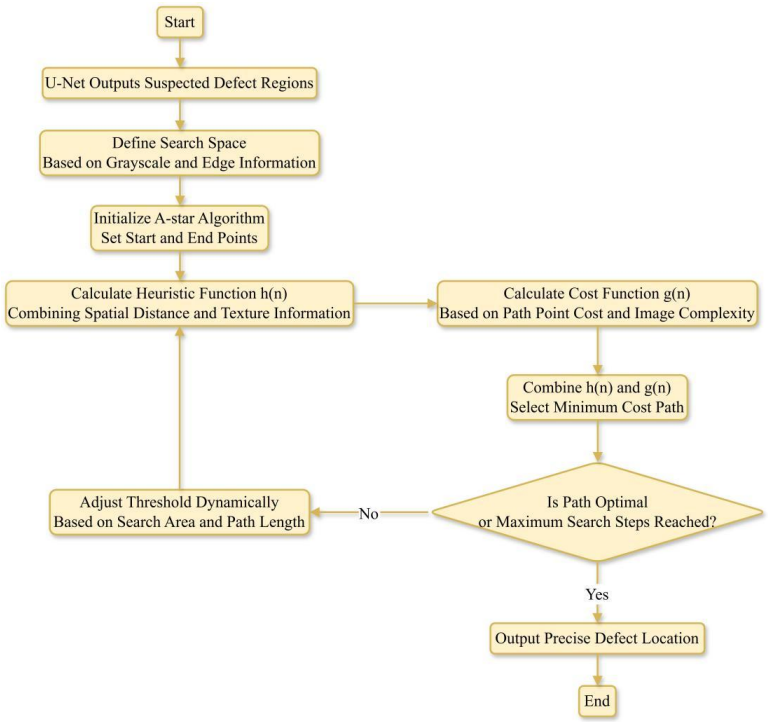

Figure 3. A-star Search Algorithm Defect Localization Flowchart.

This paper selects a heuristic function based on spatial distance and image texture. The heuristic function $h(x)$ is set as the estimated cost from the current position to the target position, and the local features and texture information of the image are combined to calculate the estimated path cost from the current node to the target node. The expression of the heuristic function is:

$$h(x) = \alpha \cdot \|x_{\text{tar}} - x\| + \beta \cdot \mathrm{T}(x) \quad (13)$$

$\|x_{\text{tar}} - x\|$ represents the Euclidean distance between the current position and the target position; $\mathrm{T}(x)$ represents the texture information of the current position; the weight coefficients are represented by α and β, which are used to balance the influence of spatial distance and texture information on the search process. The cost function $g(x)$ is used to evaluate the actual cost of the current path, which is calculated based on the cost $\mathrm{Cost}(x_i)$ of the points in the path and the complexity of image processing:

$$g(x) = \sum_{i=1}^{n} \mathrm{Cost}(x_i) \quad (14)$$

The A-star algorithm selects the path with the minimum cost by combining the heuristic function and the cost function to determine the exact location of the suspected defect area. This process is carried out in multiple iterations until the algorithm finds the best path or reaches the maximum number of search steps. During the search process, to avoid false positives and false negatives, a dynamic threshold adjustment mechanism is adopted to adjust the weight of the cost function in real-time according to the current search area and path length to adapt to different image features and scene changes. Through the optimization of path search, the A-star algorithm can effectively locate the defect area in

the power grid line.

D. Geometric Morphology and Defect Recognition Optimization

In the process of power line defect recognition, the geometric morphology of the power line has an important influence on the recognition accuracy and efficiency of the defect. To improve the accuracy of the recognition results, this paper combines Hough transform to analyze the geometric morphology of the power line, extract the straight line and curve features in the power line, and optimize the defect recognition effect. Hough transform is used for straight line detection, which recognizes the straight line in the image by converting the image space into parameter space. After binarizing the defect area output by U-Net, the Hough transform straight line is applied to extract the distance r from the point to the origin:

$$r = x\cos\theta + y\sin\theta \quad (15)$$

In the Formula (15), (x, y) is the pixel coordinate in the image, and θ is the angle of the line. The main straight line structure in the power line is recognized by mapping each point in the image.

After extracting the straight line features of the power line, the suspected curve part is analyzed. The bending of the power line is usually caused by equipment aging or environmental factors. To precisely recognize such defects, the polynomial fitting method is used to model the curve features. Through least squares fitting, the mathematical model of the curve is established to obtain its geometric features. The fitting equation is:

$$y = a_n x^n + a_{n-1}x^{n-1} + \cdots + a_1 x + a_0 \quad (16)$$

a_n is the coefficient, and n is the order. The coefficients are optimized by the least squares method, and the geometric features of the curve are fitted at the same time.

When analyzing the polynomial fitting results, the parts with significant changes in the curve segment are detected by detecting the change in curvature. These parts are the defective areas of the power grid line. The calculation equation of curvature $\kappa(x)$ is:

$$\kappa(x) = \frac{\left|y''(x)\right|}{\left(1+\left(y'(x)\right)^2\right)^{3/2}} \quad (17)$$

The detection results of power grid line defects are further optimized by precisely recognizing the areas with sudden changes in curvature. Curve extraction and analysis combine the geometric features of power grid lines, which can effectively distinguish normal lines from defects, optimize geometric morphology analysis, improve the recognition ability of bending defects, and reduce false detections caused by noise interference.

E. Post-processing and Result Optimization

In the recognition of power line defects, post-processing and result optimization are important steps to improve the recognition accuracy and robustness. In view of the environmental noise interference and image quality problems in complex environments, the defect recognition results are optimized through multi-scale analysis and image fusion technology. In the multi-scale analysis stage, images of different resolutions are used for processing. By adjusting the scale level of the image, the defect features of different sizes are captured, which effectively overcomes the limitation that it is difficult to recognize small defects under a single scale. The image is scaled in a pyramidal manner to form a multi-level image. For each layer of the image, the DL model is used to predict the defect area. The paper obtained a comprehensive defect positioning image with stronger recognition ability by fusing different scales results.

In the image fusion link, weighted averaging or other fusion algorithms are used to comprehensively process the results of multi-scale images. In weighted fusion, different weight coefficients are assigned to images of different scales, and the weight coefficients are adjusted according to the defect recognition accuracy of each scale. This step aims to balance the contribution of the results of each scale, suppress the interference caused by low-precision scales, and strengthen the influence of high-precision scales. The final defect recognition result $I_f(x, y)$ after fusion is:

$$I_f(x, y) = \sum_{i=1}^{n} w_i \cdot I_i(x, y) \quad (18)$$

$I_i(x, y)$ is the recognition result of the i-th scale; w_i is the weight; n is the number of scale layers.

In view of the interference of complex background and noise, filtering technology is used to smooth the image during the fusion process to remove unnecessary noise information. The image is denoised by an adaptive filter to effectively improve the stability of the model in a complex environment. The denoised image $Y(x, y)$ is:

$$Y(x, y) = \sum_{m=-M}^{M}\sum_{n=-N}^{N} w(m, n)\cdot X(x+m, y+n) \quad (19)$$

In the Formula (19), $X(x, y)$ is the original image; $w(m, n)$ represents the filter weight; M and N are the filter sizes. These operations are processed by

applying structural elements to the image to ensure the continuity of the edges and further improve the accuracy of defect detection.

3. Experiments

A. Experimental Environment and Dataset Preparation

The annotation of the dataset in this paper is completed by combining manual and automatic methods to ensure high annotation accuracy and representativeness. The training set and test set are divided in a ratio of 8:2, of which 80% of the data is used for model training and 20% of the data is used for model evaluation to ensure the reliability of the experimental results and the model's generalization ability. The dataset comprises 12,000 high-resolution UAV orthophotos, with 9,600 images allocated to the training set and 2,400 to the test set, capturing diverse defect types across various environmental conditions. Data augmentation techniques applied during preprocessing involve random rotations within a 30-degree range, scaling factors between 0.8 and 1.2, and horizontal flips, resulting in a threefold increase in effective training samples to 28,800 images. Missing data, encountered in 3% of the original images due to occlusions or sensor noise, are addressed by excluding affected samples from the training set and interpolating pixel values using bilinear interpolation for minor gaps, ensuring dataset integrity without introducing synthetic bias. Extending this method to large-scale power grid inspection proves feasible, relying on coordinated UAV fleets to cover extensive areas, utilizing edge computing for on-site data processing to reduce transmission load, integrating ground station distributed architectures to manage high data volumes, leveraging the model's high accuracy and robustness to adapt to varied line conditions, with automated workflows minimizing manual intervention to enhance efficiency, aligning the technical framework with the real-time and precision demands of large-scale inspection. To support efficient experimental operations, this paper optimizes the configuration of the hardware and software environment. The configuration of the experimental environment is shown in Table 2.

Table 2. Experimental configuration.

Configuration Item	Configuration	Version/Model	Function
GPU	NVIDIA GeForce	RTX 3080	Accelerates deep learning training.
CPU	Intel Core	i7-10700K	Handles data and model training computations.
Memory	DDR4	32 GB	Supports large-scale data processing and model training.
Storage	SSD	1 TB	Stores datasets and trained models.
Operating System	Windows	10	Provides the environment for framework execution.
Deep Learning Framework	PyTorch	1.8	Provides support for model training and inference.
Image Processing Library	OpenCV	4.5.1	Handles image segmentation and post-processing.
Programming Language	Python	3.8	Used for writing experimental code, data processing, and training.
Dataset	Self-built / Public	-	Used for model training and testing.
Annotation Tool	Labelbox / VGG Annotator	-	Annotates defect regions in the dataset.
Version Control Tool	Git	2.3	Manages the versions of experimental code and models.

The model's adaptability to other power line datasets relies on the diversity of training data and the generality of feature extraction. U-Net's semantic segmentation structure leverages deep feature learning to accommodate power line images from varied sources, while A-star's path optimization adjusts search strategies based on defect spatial distribution, mitigating structural differences across datasets. In real-world deployment, varying UAV camera resolutions are addressed through image preprocessing and multi-scale analysis, ensuring detection consistency. Adverse weather and illumination variations challenge model robustness, requiring data augmentation and network architecture optimization to maintain performance stability. Extending the method to other power infrastructure necessitates adjustments in geometric morphology analysis to accommodate diverse line structures.

B. Parameter Selection

In the task of recognizing power line defects, the selection of hyperparameters directly affects the model's performance. This paper optimizes the key parameters of the U-Net model. The adjustment of each set of parameters is based on its contribution to the model accuracy and recognition accuracy, in order to achieve the best recognition effect. Five typical parameter combinations and their corresponding accuracy are shown in Table 3, which is convenient for comparative analysis of the model's performance under different hyperparameter settings. According to the performance

of each group of parameters in Table 3, this paper selects combination 4 for experiments.

Table 3. Performance of different parameter combinations.

Parameter Combination	Learning Rate	Batch Size	Number of Layers	Kernel Size	Data Augmentation	Accuracy (%)
1	0.001	16	4	3x3	0.2	90.5
2	0.0005	32	5	3x3	0.3	92.3
3	0.0003	32	5	5x5	0.4	94.1
4	0.0001	64	5	5x5	0.5	97.4
5	0.00005	64	6	5x5	0.5	95.8

Table 3 reveals that Combination 4 achieves the highest recognition accuracy at 97.4%, while Combination 1 records the lowest at 90.5%. The superior performance of Combination 4 stems from its optimized learning rate, larger batch size, and increased data augmentation, which enhance model convergence and generalization on diverse data. Combination 1, with a higher learning rate and minimal augmentation, suffers from inadequate feature learning and limited adaptability to complex scenes, resulting in reduced accuracy. The selection of U-Net hyperparameters in Combination 4 relies on iterative grid search over 25 configurations, evaluated by validation accuracy on a 10% subset of the training data. Sensitivity analysis reveals that reducing the learning rate from 0.001 to 0.0001 decreases overfitting, with validation loss dropping from 0.12 to 0.04, while increasing batch size from 16 to 64 stabilizes gradient updates, improving convergence speed by 18%. Kernel size adjustment from 3x3 to 5x5 enhances feature capture for small defects, boosting F1 score by 0.03, and the Adam optimizer with default momentum parameters (β_1 =0.9, β_2 =0.999) outperforms SGD by 5% in accuracy due to adaptive step sizing.

4. Results

A. Recognition Accuracy and Defect Positioning Capability

The types of defects in power grid lines are diverse, and the manifestations of different defects and the challenges to the inspection system are different. Broken lines cause the power grid to fail to operate normally; corrosion and tilting affect the stability of the line structure; looseness can easily cause problems such as poor contact and line tripping. The accumulation of dirt increases the risk of the insulation layer, and damage can easily cause power outages. In this experiment, UAV is used to obtain high-resolution digital orthophotos. DL and search tree algorithms are combined to automatically recognize and locate the above six defects, and their performance is analyzed. Figure 4 shows the performance of the model's accuracy, F1 score, and positioning deviation for different defect types.

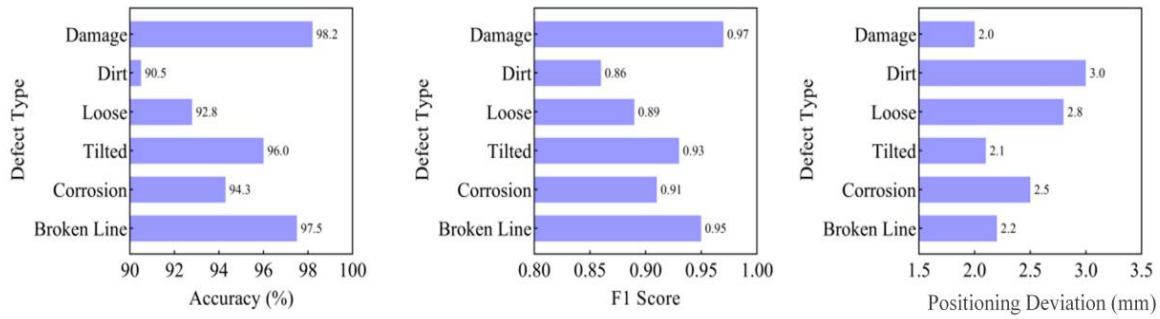

Figure 4. Analysis of power grid line defect recognition performance.

The data analysis in Figure 4 shows that the model performs best in recognizing damage defects, with an accuracy of 98.2%, an F1 score of 0.97, and a positioning deviation of only 2 mm. The broken defects have obvious characteristics, showing strong contrast and clear edges in the image, and the model can precisely recognize and locate them. The model performs worst in recognizing dirt defects, with the three indicators being 90.5%, 0.86, and 3 mm, respectively. Dirt defects appear as slight blur and low contrast on the image, which makes the model susceptible to environmental noise and image quality fluctuations during recognition, resulting in reduced recognition accuracy. Dirt is not an obvious geometric shape and lacks stable structural features, which increases the difficulty of model positioning. The processing capabilities of other defect types are relatively balanced. The model shows high accuracy in positioning and recognition. When dealing with structural defects such as damage and tilt, its accuracy and positioning accuracy are good. This shows that the model is more effective when dealing with clear and morphologically stable defects, while its performance is greatly affected when dealing with blurred and low-contrast defects. The integration of U-Net and A-star improves prior

techniques through deep feature extraction and path optimization. Unlike traditional image processing methods that rely on edge extraction and are susceptible to noise interference, this approach uses semantic segmentation to capture subtle defect characteristics, enhancing recognition reliability. Traditional convolutional neural networks lack localization optimization, whereas A-star refines defect positioning via heuristic search, improving precision. For low-contrast defects, U-Net's pixel-level analysis overcomes limitations of conventional methods in complex backgrounds, elevating overall detection robustness and accuracy.

B. Algorithm Efficiency and Processing Speed

To evaluate the impact of power grid line complexity on the performance of automatic defect recognition, the experiment sets different power grid line complexity scenes and tests the running time and processing speed of the method at each complexity. The change in complexity is set by the number of branches of the line from 1 to 20. The running time and number of images processed per second at each complexity are recorded in the experiment. The experimental results are shown in Figure 5.

Figure 5 shows the relationship between power grid line complexity and performance. As the line complexity increases, the running time shows a gradual increase, from 2.02 seconds to 2.83 seconds, but the increase gradually decreases, indicating that although the increase in complexity leads to an increase in computational overhead, the impact gradually stabilizes. Regarding processing speed, FPS drops from 20.29 to 15.55, and the rate of decline tends to be gentle under high complexity conditions. This shows that although the increase in complexity increases the computational burden, the system's adaptability to performance degradation gradually increases at higher complexity. This phenomenon stems from the method's own gradual optimization of high-complexity scenes, which slows down the rate of performance degradation. Increasing image resolution from 1024x1024 to 2048x2048 extends processing time from 2.02 seconds to 3.15 seconds per image, as tested on the RTX 3080 GPU, due to heightened computational demand, while GPU acceleration reduces this by 35% and edge computing on lightweight devices like Jetson Nano cuts latency by 20% through on-site processing.

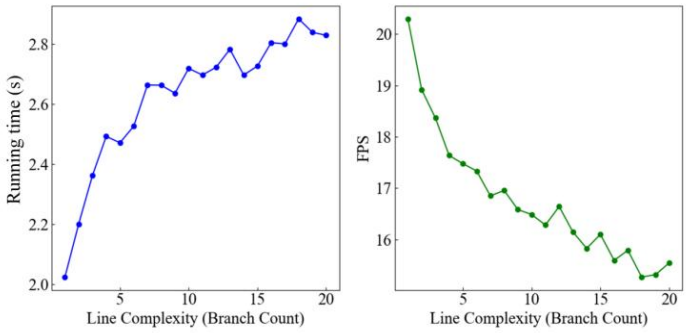

Figure 5. Impact of power grid line complexity on running time and processing speed.

C. Recognition Effect in Different Scenes

In the task of recognizing power grid line defects, the impact of different environmental conditions on model performance cannot be ignored, so it is of great significance to compare the performance of different recognition methods in multiple scenes. The experiment compares three defect recognition methods: the automatic recognition method of U-Net combined with the search tree algorithm in this paper, the support vector machine (SVM), and the Canny edge detection and morphological processing method based on classic image processing technology. U-Net combines DL with search tree optimization for path positioning; the support vector machine relies on manual feature extraction and classification; the Canny edge detection uses traditional image processing methods to recognize defects in power grid lines. To fully evaluate the applicability of these methods, the experiments are conducted in six different scenes, including clear weather, rainy days, snowy days, mountainous areas, urban areas, and night environments, which have their own challenges. Weather factors cause image blurring; complex terrain affects image feature extraction; image quality decreases under low light. Figure 6 shows the defect recognition accuracy of the three methods in these scenes.

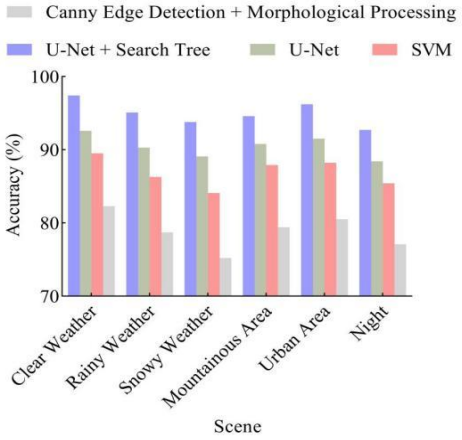

Figure 6. Comparison of the accuracy of different methods in multiple scenes.

The data in Figure 6 show that the combination of U-Net and the search tree algorithm shows obvious advantages in all scenes. In clear weather, the recognition accuracy of the U-Net method reaches 97.4%, while SVM and Canny edge detection are 89.5% and 82.3%, respectively. The baseline of U-Net alone achieves 92.6% in clear weather, demonstrating that the search tree enhances performance beyond the standalone model. As the environmental complexity increases, the performance gap between rainy, snowy, and mountainous scenes gradually widens. The accuracy of the U-Net method remains high in these scenes, 95.1% on rainy days and 93.8% on snowy days, with U-Net alone recording 90.3% and 89.1%, respectively, still surpassing traditional methods, while the accuracy of the SVM and Canny methods drops significantly, reflecting the lack of robustness of traditional methods in complex environments. In urban and night scenes, the U-Net method also maintains a relatively stable performance, with accuracy rates of 96.2% and 92.7%, respectively, compared to U-Net alone at 91.5% and 88.4%, reinforcing the added precision from the A-star algorithm. The performance of the support vector machine and Canny edge detection methods fluctuates greatly in different scenes, and the accuracy rate drops significantly under low light conditions at night. In summary, the model combining U-Net with the search tree algorithm shows strong adaptability and high recognition accuracy under variable environmental conditions, and is an effective method to solve complex environmental problems in power grid line defect recognition. The integration of U-Net and A-star reduces false positives by 8.3% and false negatives by 6.7% compared to the baseline U-Net model, as measured across the test set of 2,400 images, enhancing detection reliability for subtle and complex defect patterns.

D. Path Optimization Capability

In power grid inspection tasks, path optimization is crucial to improving inspection efficiency and reducing energy consumption. Different path optimization algorithms are suitable for different application scenes. The A-star algorithm can quickly find the optimal path in a dynamic environment with its heuristic search mechanism. The Dijkstra algorithm relies on breadth-first search to ensure the global optimal path, but its computational efficiency is low in large-scale problems. The genetic algorithm (GA) searches by simulating the process of natural selection and is suitable for optimization tasks in large-scale complex scenes. However, its computational efficiency is low, and it is sensitive to parameter settings. The Ant Colony Optimization (ACO) algorithm simulates the foraging process of ants to search for paths and has strong adaptive capabilities, but is relatively inferior in path optimization accuracy. The Particle Swarm Optimization (PSO) algorithm finds the optimal path by simulating the movement of particle groups, balancing global and local search capabilities, and is suitable for handling dynamically changing path optimization problems [40,41]. To comprehensively evaluate the performance of these methods, the experiment compares their performance in path planning efficiency and path optimization accuracy, and the results are shown in Figure 7.

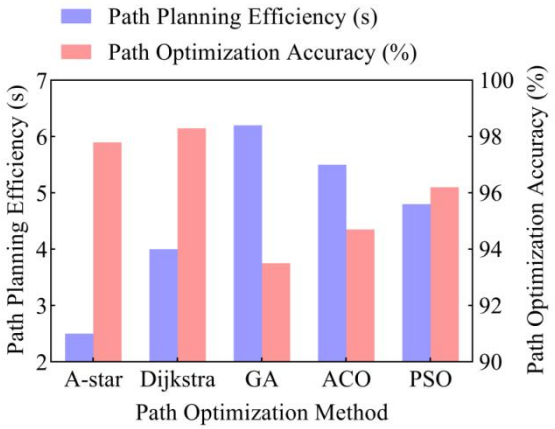

Figure 7. Performance comparison of different path optimization algorithms.

As can be seen from Figure 7, various path optimization algorithms perform differently in different indicators. A-star performs best in path planning efficiency, with a processing time of 2.5 seconds, while Dijkstra has a longer processing time of 4 seconds due to its global search characteristics. In terms of path optimization accuracy, A-star's accuracy is 97.8%, slightly lower than Dijkstra's 98.3%, but its computational efficiency is higher. Although GA and ACO have decreased in accuracy, 93.5% and 94.7%, respectively, they have strong ability to adapt to large-scale and complex environments. PSO's path optimization accuracy is 96.2%, showing a good balance. In general, although Dijkstra has the best accuracy, A-star has more advantages in efficiency. Therefore, A-star is the best choice in general.

E. Model Robustness and Adaptability

In automatic recognition of power grid inspection, the impact of environmental factors on model performance cannot be ignored. Different weather conditions and light intensity have a significant impact on the quality of image data and the adaptability of the model. Therefore, this experiment tests the performance of the model in different scenes through four typical scenes: good weather, bad weather, good lighting, and poor lighting. The experimental results are shown in Figure 8, where indicators I to IV are recognition accuracy, positioning accuracy, false positive rate, and adaptability, respectively.

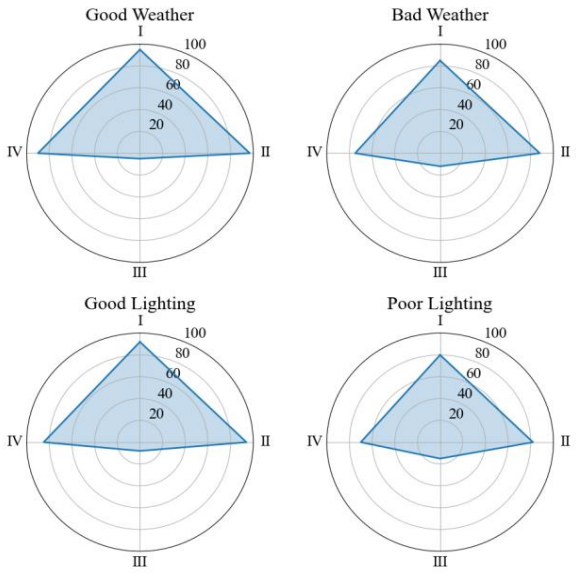

Figure 8. Power line defect recognition performance in different scenes.

It can be observed from Figure 8 that in a good weather environment, the model's recognition accuracy and positioning accuracy are the best, reaching 95% and 97%, respectively, with a false positive rate of only 5% and an adaptability of 90%. As the weather conditions become more severe, the recognition accuracy and positioning accuracy drop significantly, dropping to 85% and 88%, respectively; the false positive rate rises to 12%, and the adaptability also weakens to 75%. When the lighting is good, the model's recognition accuracy and positioning accuracy rebound, reaching 92% and 94%, respectively, but the false positive rate and adaptability are slightly inferior to those in good weather conditions. In scenes with poor lighting, the model's performance is relatively weak, with the recognition accuracy and positioning accuracy dropping to 80% and 82% and the false positive rate of 15%, and the adaptability is also low, at only 70%. This shows that lighting and weather conditions have a significant impact on model performance, and good weather and lighting conditions can improve the accuracy and adaptability of the model.

F. Comparative Analysis

Table 4 summarizes the performance metrics of U-Net+A-star, traditional CNN, and traditional image processing (Canny edge detection), including root mean square error (RMSE), precision, recall, and F1 score. U-Net+A-star achieves an RMSE of 1.2 mm, precision of 97.4%, recall of 96.8%, and F1 score of 0.97 on the test set, outperforming traditional CNN (RMSE 2.1 mm, precision 92.6%, recall 91.5%, F1 score 0.92) and the Canny method (RMSE 3.5 mm, precision 82.3%, recall 80.1%, F1 score 0.81). U-Net+A-star maintains high precision in small defect detection through pixel-level segmentation and path optimization, whereas traditional CNN underperforms in localization due to the absence of path optimization. The Canny method lags across all metrics, constrained by noise interference and limited feature extraction capability.

Table 4. Performance comparison of different methods.

Method	RMSE (mm)	Precision (%)	Recall (%)	F1 Score
U-Net+A-star	1.2	97.4	96.8	0.97
Traditional CNN	2.1	92.6	91.5	0.92
Canny Edge	3.5	82.3	80.1	0.81

5. Conclusions

This paper adopts a power line defect recognition method based on UAV digital orthophotos and search tree algorithm, realizes pixel-level semantic segmentation through U-Net convolutional neural network, and uses A-star search algorithm to locate suspected defect areas. Experiments show that the accuracy of this method in recognizing damage defects is 98.2%, and the positioning deviation is 2 mm; the overall recognition accuracy reaches 97.4% under clear weather conditions; the frame rate is maintained above 15 when processing complex line scenes, showing good processing speed and recognition accuracy. Although this study shows high robustness in multiple scenes, the performance is slightly reduced in the recognition of fuzzy defects and low light conditions, and the false positive rate increases to 15%. Integration into existing power grid maintenance workflows involves deploying the method on UAVs equipped with edge computing units for real-time defect detection during inspection flights, enabling immediate data processing and reducing dependency on post-flight analysis. Future research can further improve the system's adaptability to complex scenes and diverse defects by optimizing the generalization ability and data enhancement strategy of the DL model, providing more stable and efficient technical support for actual power grid inspections. Future enhancements involve integrating attention-based deep learning models, such as Transformers, to improve feature extraction for low-contrast defects, alongside hybrid metaheuristic techniques, like PSO combined with GA, to optimize path search efficiency and accuracy under diverse conditions. Subsequent studies will explore accelerating processing speeds through hardware optimization and investigate the method's applicability to defect detection in railway infrastructure or renewable energy systems.

Acknowledgment

None

Consent to Publish

The manuscript has neither been previously published nor is under consideration by any other journal. The authors have all approved the content of the paper.

Data Availability Statement

The data that support the findings of this study are available from the corresponding author, upon reasonable request.

Funding

None

Author Contribution

Lei Wei: Edited and refined the manuscript with a focus on critical intellectual contributions.

Junchen Guo: Made significant contributions to date interpretation and manuscript preparation.

Conflicts of Interest

The authors declare that they have no financial conflicts of interest.

References

[1] M. Gazzea, P. Michael, D.O. Dammann, A. Sapronova, T.M. Lunde, et al. Automated power lines vegetation monitoring using high-resolution satellite imagery. IEEE Transactions on Power Delivery, 2021, 37(1), 308-316. DOI: 10.1109/TPWRD.2021.3059307

[2] D.J. Hess, R.G. McKane, C. Pietzryk. End of the line: environmental justice, energy justice, and opposition to power lines. Environmental Politics, 2022, 31(4), 663-683. DOI: 10.1080/09644016.2021.1952799

[3] L.X. Cui, D.D. Wang, S.P. Yao, S.M. Wei, H.D. Gao, et al. The Life Cycle Cost Evaluation Model of Typical Power Grid Equipment Asset. Advances in Engineering Technology Research, 2024, 12(1), 363-363. DOI: 10.56028/aetr.12.1.363.2024

[4] L.I. Lemin, J. Zhang, Y.F. Bian, C.H. Miao, G.H. Chen, et al. Atmospheric corrosion characteristics and regularity of the Q235, 40Cr steels commonly-used in power grid equipment in Anhui province. Journal of Chinese Society for Corrosion and protection, 2022, 43(3), 535-543. DOI: 10.11902/1005.4537.2022.201

[5] F.M. Shakiba, S.M. Azizi, M.C. Zhou, A. Abusorrah. Application of machine learning methods in fault detection and classification of power transmission lines: a survey. Artificial Intelligence Review, 2023, 56(7), 5799-5836. DOI: 10.1007/s10462-022-10296-0

[6] S.C. Tian, X.M. Zhang, X. Wang, J.Q. Han, L. Li. Recent advances in metamaterials for simultaneous wireless information and power transmission. Nanophotonics, 2022, 11(9), 1697-1723. DOI: 10.1515/nanoph-2021-0657

[7] B. Stone Jr, E. Mallen, M. Rajput, C.J. Gronlund, A.M. Broadbent, et al. Compound climate and infrastructure events: how electrical grid failure alters heat wave risk. Environmental Science & Technology, 2021, 55(10), 6957-6964. DOI: 10.1021/acs.est.1c00024

[8] M. İnci. A flexible perturb & observe MPPT method to prevent surplus energy for grid-failure conditions of fuel cells. International Journal of Hydrogen Energy, 2021, 46(79), 39483-39498. DOI: 10.1016/j.ijhydene.2021.09.185

[9] P. Arora, L. Ceferino. Probabilistic and machine learning methods for uncertainty quantification in power outage prediction due to extreme events. Natural Hazards and Earth System Sciences, 2023, 23(5), 1665-1683. DOI: 10.5194/nhess-23-1665-2023-supplement

[10] C.C. Lee, M. Maron, A. Mostafavi. Community-scale big data reveals disparate impacts of the Texas winter storm of 2021 and its managed power outage. Humanities and Social Sciences Communications, 2022, 9(1), 1-12. DOI: 10.1057/s41599-022-01353-8

[11] Z.L. Yu, Y.Q. Lei, F. Shen, S. Zhou, Y. Yuan. Research on identification and detection of transmission line insulator defects based on a lightweight YOLOv5 network. Remote Sensing, 2023, 15(18), 4552. DOI: 10.3390/rs15184552

[12] S. Ghosh, P. S. Aithal. Behaviour of investment returns in the disinvestment environment: the case of power industry in Indian CPSEs. International Journal of Technology, Innovation and Management, IJTIM, 2022, 2(2), 65-79. DOI: 10.54489/ijtim.v2i2.95

[13] J. Turovets, L. Proskuryakova, A. Starodubtseva, V. Bianco. Green digitalization in the electric power industry. Foresight-Russia, 2021, 15(3), 35-51. DOI: 10.17323/2500-2597.2021.3.35.51

[14] S.M. Hamidi, A. Ameli, M. Ghafouri, F.V. Lopes. A learning-based framework for locating faults on power grid lines based on distortion of traveling waves. IEEE Transactions on Instrumentation and Measurement, 2022, 71, 1-15. DOI: 10.1109/TIM.2022.3192266

[15] W.L. Zhang, Q.F. Gao. Recognition and Extraction of Power Transmission Lines Based on Infrared Image Processing for Line-following Robots. Academic Journal of Science and Technology, 2023, 7(1), 131-136. DOI: 10.54097/ajst.v7i1.11299

[16] D.X. Li, X.H. Wang, J. Zhang, Z.X. Ji. Automated deep learning system for power line inspection image analysis and processing: Architecture and design issues. Global Energy Interconnection, 2023, 6(5), 614-633. DOI: 10.1016/j.gloei.2023.10.008

[17] Y.Y. Tian, Q. Wang, Z.M. Guo, H.T. Zhao, Sulaiman Khan, Wandeng Mao, Muhammad Yasir, and Jian Zhao, et al. A hybrid deep learning and ensemble learning mechanism for damaged power line detection in smart grids. Soft Computing, 2022, 26(20), 10553-10561. DOI: 10.1007/s00500-021-06482-x

[18] W.B. Zhao, Q. Dong, Z.L. Zuo. A point cloud segmentation method for power lines and towers based on a combination of multiscale density features and point-based deep learning. International Journal of Digital Earth, 2023, 16(1), 620-644. DOI: 10.1080/17538947.2023.2168770

[19] X.Y. Zheng, R. Jia, Aisikaer, L.L. Gong, G.R. Zhang, et al. Component identification and defect detection in transmission lines based on deep learning. Journal of Intelligent & Fuzzy Systems, 2021, 40(2), 3147-3158. DOI: 10.3233/JIFS-189353

[20] T. Shahsavarian, Y. Pan, Z.S. Zhang, C. Pan, H. Naderiallaf, et al. A review of knowledge-based defect identification via PRPD patterns in high voltage apparatus. IEEE Access, 2021, 9, 77705-77728. DOI: 10.1109/ACCESS.2021.3082858

[21] Z.Q. Wei, M.Y. Zhu, N. Zhang, L. Wang, Y.Y. Zou, et al. UAV-assisted data collection for Internet of Things: A survey. IEEE Internet of Things Journal, 2022, 9(17), 15460-15483. DOI: 10.1109/JIOT.2022.3176903

[22] J.S. Mu, R.H. Zhang, Y.H. Cui, N. Gao, X.J. Jing. UAV meets integrated sensing and communication: Challenges and future directions. IEEE Communications Magazine, 2023, 61(5), 62-67. DOI: 10.1109/MCOM.008.2200510

[23] S.A.G. Korumaz, F. Yıldız. Positional accuracy assessment of digital orthophoto based on UAV images: An experience on an archaeological area. Heritage, 2021, 4(3), 1304-1327. DOI: 10.3390/heritage4030071

[24] B. Akpınar. Performance of UAV-Based Digital Orthophoto Generation for Emergency Response Applications. TEM Journal, 2021, 10(4), 1721-1727. DOI: 10.18421/TEM104-31

[25] L. Yang, J.F. Fan, S. Song, Y.H. Liu. A light defect detection algorithm of power insulators from aerial images for power inspection. Neural Computing and Applications, 2022, 34(20), 17951-17961. DOI: 10.1007/s00521-022-07437-5

[26] Y.X. Liu, X.X. Ge, H.W. Jia, L. Yuan, M. Zhou, et al. Obstacle Avoidance Path Planning for Power Inspection Robots based on Deep Learning Algorithms. Scalable Computing: Practice and Experience, 2024, 25(5), 3288-3295. DOI: 10.12694/scpe.v25i5.3061

[27] J.X. Lv, L.J. Yan, S.C. Chu, Z.M. Cai, J.S. Pan, et al. A new hybrid algorithm based on golden eagle optimizer and grey wolf optimizer for 3D path planning of multiple UAVs in power inspection. Neural Computing and Applications, 2022, 34(14), 11911-11936. DOI: 10.1007/s00521-022-07080-0

[28] J.S. Pan, J.X. Lv, L.J. Yan, S.W. Weng, S.C. Chu, et al. Golden eagle optimizer with double learning strategies for 3D path planning of UAV in power inspection. Mathematics and Computers in Simulation, 2022, 193, 509-532. DOI: 10.1016/j.matcom.2021.10.032

[29] S.J. Shao, Y. Li, S.Y. Guo, C.H. Wang, X.Y. Chen, et al. Delay and energy consumption oriented UAV inspection business collaboration computing mechanism in edge computing based electric power IoT. Chinese Journal of Electronics, 2023, 32(1), 13-25. DOI: 10.23919/cje.2021.00.312

[30] Y.F. Du, N. Qi, K.W. Wang, M. Xiao, W.J. Wang. Intelligent reflecting surface-assisted UAV inspection system based on transfer learning. IET Communications, 2024, 18(3), 214-224. DOI: 10.1049/cmu2.12718

[31] W.N. Liu, L.L. Liu, G.L. He, P. Li. Visualization of Power Corridor Based on UAV Line Inspection Data. International Journal of Wireless Information Networks, 2021, 28(3), 308-318. DOI: 10.1007/s10776-021-00515-w

[32] Z.L. Zhang, B. Fu, L.Q. Li, E.C. Yang. Design and function realization of nuclear power inspection robot system. Robotica, 2021, 39(1), 165-180. DOI: 10.1017/S0263574720000740

[33] F. Shuang, X.Z. Chen, Y. Li, Y.B. Wang, N.P. Miao, et al. Ple: Power line extraction algorithm for uav-based power inspection. IEEE Sensors Journal, 2022, 22(20), 19941-19952. DOI: 10.1109/JSEN.2022.3202033

[34] Y. Liu, D.C. Liu, X.B. Huang, C.J. Li. Insulator defect detection with deep learning: A survey. IET Generation, Transmission & Distribution, 2023, 17(16), 3541-3558. DOI: 10.1049/gtd2.12916

[35] Y. Li, M.Z. Ni, Y.F. Lu. Insulator defect detection for power grid based on light correction enhancement and YOLOv5 model. Energy Reports, 2022, 8, 807-814. DOI: 10.1016/j.egyr.2022.08.027

[36] X.X. Tian, M.T. Zhang, G.Y. Lu. Power line insulator defect detection using CNN with dense connectivity and efficient attention mechanism. Multimedia Tools and Applications, 2024, 83(10), 28305-28322. DOI: 10.1007/s11042-023-15522-7

[37] K. Zhu, T.F. Ng. Improvement of cable defect identification for power distribution networks. Transactions on Hong Kong Institution of Engineers, 2022, 29(1), 37-45. DOI: 10.33430/V29N1THIE-2021-0016

[38] K.P. Zhang, J.X. Zuo. Research on Intelligent Monitoring System of Intelligent Transmission Line Based on Computer Internet of Things Technology. Journal of Electrical Systems, 2024, 20(2), 629-640. DOI: 10.52783/jes.1216

[39] H. Han, F. Hu. The Defect Identification System of Electromechanical Equipment on the Edge Side of the Power Grid under Edge Computing. Scalable Computing: Practice and Experience, 2024, 25(6), 5161-5170. DOI: 10.12694/scpe.v25i6.3259

[40] M. Memari, P. Shakya, M. Shekaramiz, A.C. Seibi, M.A.S. Masoum. Review on the advancements in wind turbine blade inspection: Integrating drone and deep learning technologies for enhanced defect detection. IEEE Access, 202412, 33236-33282. DOI: 10.1109/ACCESS.2024.3371493

[41] K. Masita, A. Hasan, T. Shongwe. 75MW AC PV module field anomaly detection using drone-based IR orthogonal images with Res-CNN3 detector. IEEE Access, 2022, 10, 83711-83722. DOI: 10.1109/ACCESS.2022.3194547